

Quantum criticality in the two-channel pseudogap Anderson model: A test of the non-crossing approximation

Farzaneh Zamani,^{*,1,2} Tathagata Chowdhury,³ Pedro Ribeiro,^{1,2} Kevin Ingersent,³ Stefan Kirchner^{1,2}

¹ Max Planck Institute for the Physics of Complex Systems, Nöthnitzer Str. 38, D-01187 Dresden, Germany

² Max Planck Institute for Chemical Physics of Solids, Nöthnitzer Str. 40, D-01187 Dresden, Germany

³ Department of Physics, University of Florida, Gainesville, Florida 32611-8440, USA

Received XXXX, revised XXXX, accepted XXXX

Published online XXXX

Key words: Quantum criticality, Anderson model, two-channel, pseudogap, NCA, NRG, scaling.

* Corresponding author: e-mail farzaneh@pks.mpg.de, Phone: +49-351-871-1128

We investigate the dynamical properties of the two-channel Anderson model using the noncrossing approximation (NCA) supplemented by numerical renormalization-group calculations. We provide evidence supporting the conventional wisdom that the NCA gives reliable results for the standard two-channel Anderson model of a magnetic impurity in a metal. We extend the analysis to the pseudogap two-channel model describing a semi-metallic host with a density of states that vanishes in power-law fashion at the Fermi energy.

This model exhibits continuous quantum phase transitions between weak- and strong-coupling phases. The NCA is shown to reproduce the correct qualitative features of the pseudogap model, including the phase diagram, and to yield critical exponents in excellent agreement with the NRG and exact results. The forms of the dynamical magnetic susceptibility and impurity Green's function at the fixed points are suggestive of frequency-over-temperature scaling.

Copyright line will be provided by the publisher

1 Introduction Quantum criticality is currently pursued across many areas of correlated matter, from insulating or weak magnets to metal-insulator systems to unconventional superconductors. Interest in continuous phase transitions at temperature $T = 0$ is motivated both by the appearance of novel phases near such transitions and by a richness of quantum critical states that extends beyond the traditional description in terms of order-parameter fluctuations. A fertile area for experimental study has been the border of magnetism in rare-earth and actinide intermetallics, where there is mounting evidence that a crucial issue is the fate of the Kondo effect on approach to the quantum phase transition [1, 2]: if Kondo screening becomes critical concomitantly with the bulk magnetization, then dynamical scaling ensues, signaling the absence of additional energy scales at criticality [3, 4].

This paper investigates critical Kondo destruction and dynamical scaling in the pseudogap two-channel Anderson model. We focus on the treatment of the problem using the noncrossing approximation (NCA), which involves a self-consistent evaluation of all irreducible self-energy diagrams without vertex corrections. Within a pseudoparticle representation of the impurity spin [5], the NCA threshold exponents of the $T = 0$ pseudoparticle propagators for the one-channel Anderson model [6] are known to differ from the correct exponents inferred from Friedel's sum rule [7]. In contrast, the NCA threshold exponents for multichannel Anderson models agree [8] with those predicted by boundary conformal field theory [9, 10]. The NCA is therefore believed to work well for this model, which has been studied extensively as a relatively simple route to non-Fermi liquid behavior. The pseudogap version of the two-channel Kondo model, in which the host density of states vanishes

Copyright line will be provided by the publisher

in power-law fashion at the Fermi energy, was first studied in Ref. [11]. The model and the counterpart Anderson model have attracted renewed interest [12] due to proposals [13, 14] of their realization in the context of adatoms on graphene, where the band structure gives rise to two symmetry-inequivalent Dirac points. Recent scanning tunneling spectroscopy data are in line with expectations for pseudogap multichannel Kondo physics [15].

Here we briefly revisit the reliability of the NCA for the metallic two-channel Anderson model before turning to the pseudogap case, where we apply a scaling ansatz to obtain $T = 0$ threshold exponents, and hence extract critical exponents describing physical properties. We find good agreement between these exponents and ones obtained using full numerical solutions of the NCA equations at $T > 0$ and using the numerical renormalization group.

2 The pseudogap M-channel Anderson model

The $SU(N) \times SU(M)$ Anderson model can be written

$$H_{MCA} = \sum_{\mathbf{k}} \sum_{\sigma=1}^N \sum_{\mu=1}^M \epsilon_{\mathbf{k}} c_{\mathbf{k}\sigma\mu}^\dagger c_{\mathbf{k}\sigma\mu} + \epsilon_f \sum_{\sigma} f_{\sigma}^\dagger f_{\sigma} + V \sum_{\mathbf{k}, \sigma, \mu} \left(c_{\mathbf{k}\sigma\mu}^\dagger f_{\sigma} b_{\mu}^\dagger + \text{H.c.} \right), \quad (1)$$

where $c_{\mathbf{k}\sigma\mu}^\dagger$ creates a conduction electron of wave vector \mathbf{k} in channel μ and spin projection σ . The representation $d_{\sigma\mu}^\dagger = f_{\sigma}^\dagger b_{\mu}^\dagger$ of the impurity electron creation operator in terms of pseudofermion creation combined with slave-boson annihilation faithfully reproduces the $SU(N) \times SU(M)$ Anderson model provided that the constraint $Q = \sum_{\sigma} f_{\sigma}^\dagger f_{\sigma} + \sum_{\mu} b_{\mu}^\dagger b_{\mu} = 1$ is enforced exactly.

We assume a conduction-electron density of states

$$\rho(\omega) = -\frac{1}{\pi} \text{Im} G_c(\omega) = \frac{r+1}{2D^{r+1}} |\omega|^r \Theta(D - |\omega|) \quad (2)$$

that vanishes at the Fermi energy $\omega = 0$ in a manner governed by exponent r , taken to satisfy $0 < r < 1$; the special case $r = 0$ describes a flat (metallic) band. The half-bandwidth D acts as the basic energy scale in the problem.

$N = 2$ and $M = 1$, Eq. (1) reduces to the standard Anderson impurity model (with infinite on-site Coulomb repulsion) which in turn contains the spin-isotropic Kondo model as an effective low-energy model, while for $N \rightarrow \infty$ various saddle-point approximations can be constructed [16, 8, 17]. The dynamical large- N limit of Ref. [17] for the spin-isotropic Kondo model uses a generating functional equivalent to that for the NCA, making it seem natural to expect similar results from the two approaches. However, it is important to note that within NCA, the slave-boson propagator $G_b(\omega)$ is not a Hubbard-Stratonovich decoupling field and is therefore dynamic even at the bare level, and that $G_b(\omega)$ couples to the local constraint, which is enforced exactly. As a consequence, $G_b(\omega)$ and the pseudofermion propagator $G_f(\omega)$ in the NCA develop threshold behavior reminiscent of the core hole propagator in the

x-ray edge problem, resulting in maximally particle-hole asymmetric spectral functions: $\text{Im } G_b(\omega \rightarrow 0, T = 0) \sim \Theta(\omega) |\omega|^{-\alpha_b}$ and $\text{Im } G_f(\omega \rightarrow 0, T = 0) \sim \Theta(\omega) |\omega|^{-\alpha_f}$. Therefore, $G_b(\tau, T)$ and $G_f(\tau, T)$ should be rather different from their dynamical large- N counterparts, raising the question of whether dynamical or ω/T scaling—a property that arises naturally within the dynamical large- N approach—can carry over to the NCA.

3 Asymptotically exact zero-temperature solution For the case $r = 0$ of a constant density of conduction-electron states, an exact finite-temperature solution can be obtained by transforming the NCA's integral equations into a set of coupled differential equations [6]. As this procedure relies on specific properties of the NCA solution for $r = 0$, its extension to the pseudogap case is unclear. We can address the zero-temperature form of the NCA solution by imposing a scaling ansatz for the pseudoparticle spectral functions. The scaling ansatz has been successfully used to extract critical properties of impurity models treated within the dynamical large- N approximation, including the Kondo model both with a metallic ($r = 0$) density of states [17] and with a pseudogap [18], the Bose-Fermi Kondo model [19], and the pseudogap Bose-Fermi Kondo model [20]. Here we show that a generalization of this ansatz to the case of extreme particle-hole asymmetry (generated by the exact enforcement of the constraint) can be used to extract the critical properties of the fixed points within the NCA.

The NCA self-energies for the pseudoparticle propagators at real frequencies are [21, 22]

$$\Sigma_{f\sigma}^{\text{ret}}(\omega) = V^2 \sum_{\mu} \int d\epsilon f(\epsilon) A_{c\sigma\mu}(-\epsilon) G_b^{\text{ret}}(\epsilon + \omega), \quad (3)$$

$$\Sigma_{b\mu}^{\text{ret}}(\omega) = V^2 \sum_{\sigma} \int d\epsilon f(\epsilon) A_{c\sigma\mu}(\epsilon) G_f^{\text{ret}}(\epsilon + \omega), \quad (4)$$

where the superscript “ret” specifies a retarded function, $A_{c\sigma\mu}(\omega) = -\pi^{-1} \text{Im } G_{c\sigma\mu}^{\text{ret}}(\omega) = \rho(\omega)$, and $f(\epsilon)$ is the Fermi-Dirac distribution function. Working at temperature $T = 0$, we make the ansatz [23, 7]

$$A_p(\omega) = a_p \Theta(\omega) \omega^{-\alpha_p}, \quad p = f, b, \quad (5)$$

for the pseudoparticle spectral functions $A_p(\omega) = -\pi^{-1} \text{Im } G_p^{\text{ret}}(\omega)$, with α_p being a threshold exponent and a_p a constant. Substituting these scaling forms into Eqs. (3) and (4), and applying Dyson's equations, one obtains the self-consistency conditions

$$\alpha_f + \alpha_b = 1 + r, \quad (6)$$

$$\sin(\pi\alpha_f) \sin[\pi(r - \alpha_f)] \times \left\{ \frac{M}{N} \frac{\sin[\pi(r - \alpha_f)]}{\alpha_f} + \frac{\sin(\pi\alpha_f)}{1 + r - \alpha_f} \right\} = 0. \quad (7)$$

Equation (6) is obtained by matching exponents and Eq. (7) by matching amplitudes. Hereafter, we focus on the

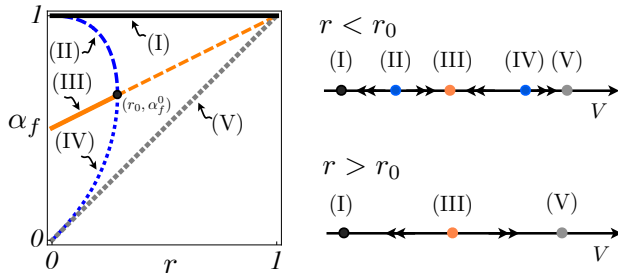


Figure 1 Left: Variation with pseudogap exponent r of possible solutions α_f of Eq. (7) for the two-channel Anderson model. Dashed lines represent unstable fixed points and dotted lines show values not observed in numerical solutions of the finite-temperature NCA equations. Right: Renormalization-group (RG) flows and fixed points as functions of hybridization V for the ranges $0 < r < r_0$ and $r > r_0$. Labels (I)–(V) connect RG fixed points with NCA solutions in the left panel.

two-channel case $N = M = 2$, for which the possible solutions of Eqs. (6) and (7) are plotted schematically on the r - α_f plane in Fig. 1. For $r = 0$, the solutions are $\alpha_f = 0$, $\alpha_f = 1$ (local moment), and $\alpha_f = \frac{1}{2}$ (intermediate coupling), in agreement with Ref. [7]. For $0 < r < r_0$, where the condition $(r_0 + 1)\pi/2 = \cot(r_0\pi/2)$ yields a numerical value $r_0 \simeq 0.292$, there are five solutions, of which three correspond to stable renormalization-group fixed points: local moment (I), two-channel Kondo (III), and infinite- U resonant level (V). For $r > r_0$, there are just three solutions, of which only (I) and (V) are stable.

The (physical) impurity Green’s function is obtained as

$$G_{d\sigma\mu}^{\text{ret}}(\omega) = \int d\epsilon e^{-\beta\epsilon} [G_{f\sigma}^{\text{ret}}(\epsilon + \omega) A_{b\mu}(\epsilon) - G_{b\mu}^{\text{adv}}(\epsilon - \omega) A_{f\sigma}(\epsilon)], \quad (8)$$

where $\beta = 1/T$ and “adv” means advanced. The $T = 0$ scaling form of this Green’s function and of the local spin susceptibility χ can be deduced from the pseudoparticle propagators by simple arguments, yielding $\text{Im } G_d^{\text{ret}}(\omega) \propto |\omega|^{1-\alpha_f-\alpha_b} \equiv |\omega|^{-r}$ and $\text{Im } \chi(\omega) \propto \text{sgn}(\omega) |\omega|^{1-2\alpha_f}$.

The NRG has been applied previously to the pseudogap two-channel Kondo model [11, 12]. For $r < r_{\text{max}} \simeq 0.23$ (somewhat smaller than the NCA value $r_0 \simeq 0.292$), the method finds three stable fixed points separated by two unstable critical points, precisely analogous to the situation shown in Fig. 1. For $r_{\text{max}} < r < 1$, the NRG yields one critical point between two stable fixed points, again in one-to-one agreement with the NCA scaling ansatz. Of these fixed points, only those corresponding to (I)–(III) can be accessed for level energies $\epsilon_f < 0$, the regime considered in the present paper. (The NCA treatment of cases with $\epsilon_f > 0$ will be reported elsewhere [20].)

We have confirmed that the pseudogap two-channel Anderson model shares the same fixed points and criti-

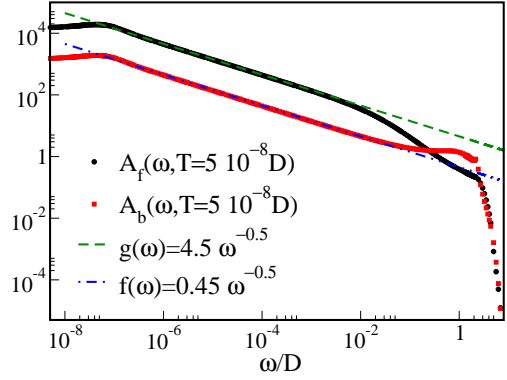


Figure 2 Pseudoparticle spectral functions $A_f(\omega)$ and $A_b(\omega)$ for a metallic host ($r = 0$), calculated at temperature $T = 5 \times 10^{-8} D$ for $\epsilon_f/D = -0.6$ and $(V/D)^2 = 0.5$. The NCA pseudoparticle threshold exponents $\alpha_f = \alpha_b = 0.5$ agree with the exactly known results.

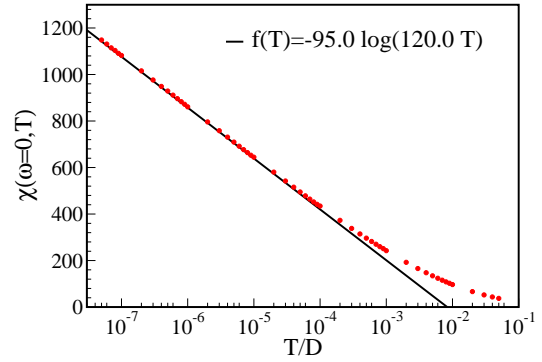


Figure 3 Static susceptibility χ vs temperature T for a metallic host ($r = 0$) and $\epsilon_f/D = -0.6$, $(V/D)^2 = 0.5$. The NCA captures the logarithmic divergence of $\chi(T)$.

cal properties as its Kondo counterpart, in agreement with the conclusions of Ref. [12]. This justifies our comparisons below between NCA results for the Anderson model and NRG results for the Kondo model (the smaller Hilbert space of which allows greater numerical efficiency).

4 Finite-temperature NCA solution At temperatures $T > 0$, the NCA equations are amenable to a numerical solution on the real frequency axis over a wide parameter range. Details of the numerical evaluation scheme can be found, *e.g.*, in [24].

Results for $r = 0$: As mentioned above, the NCA predicts the correct threshold exponents for multichannel Anderson models with a metallic density of states. This is illustrated in Fig. 2, where the fitted pseudoparticle exponents agree very well with the NCA scaling ansatz and with the boundary conformal field theory for the two-channel Kondo model [25]. Figure 3 demonstrates that the NCA correctly captures the logarithmic divergence in temper-

	(I)	(II)	(III)	(IV)	(V)
α_f	1.0	0.967	0.575	0.183	0.15
α_b	0.15	0.183	0.575	0.967	1.0

Table 1 Pseudoparticle threshold exponents at $T = 0$ for the two-channel Anderson model with $r = 0.15$.

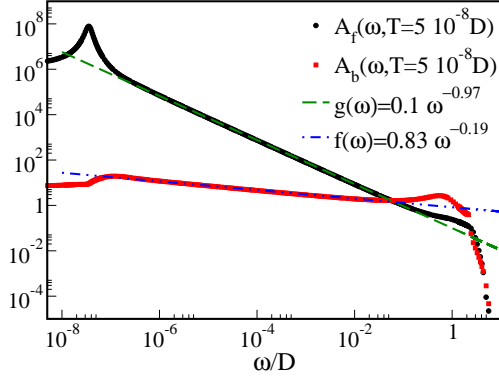


Figure 4 Pseudoparticle spectral functions $A_f(\omega)$ and $A_b(\omega)$ for $r = 0.15$, $T = 5 \times 10^{-8}D$, $\epsilon_f/D = -0.6$, and $(V/D)^2 = 0.27$. The power-law behaviors correspond to solution (II) in Table 1 and Fig. 1.

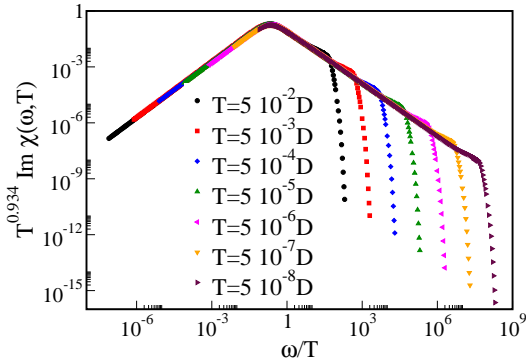


Figure 5 Dynamical scaling of $\chi(\omega, T)$ at the critical fixed point (II) in Fig. 1, for $r = 0.15$, $\epsilon_f/D = -0.6$, and $(V/D)^2 = 0.27$.

ature T of the local spin susceptibility χ . The subleading behavior of the impurity spectral function, $A_d(\omega) \equiv -\pi^{-1} \text{Im } G_d^{\text{ret}}$, is also reproduced [8]: $A_d(\omega) - A_d(0) \sim \sqrt{|\omega|}$. Taken together, these pieces of evidence indicate that the NCA gives qualitatively correct results for the $r = 0$ two-channel Anderson problem.

Results for $r = 0.15$: We now turn to numerical results for the two-channel pseudogap Anderson model, focusing first on the case $r = 0.15$ with $\epsilon_f = -0.6D$ as a representative example of the behavior in the range of pseudogap exponents $0 < r < r_0$. For this case, Eqs. (6) and (7) predict five solutions, listed in Table 1. Solution (I) corresponds to the local-moment fixed point where V effec-

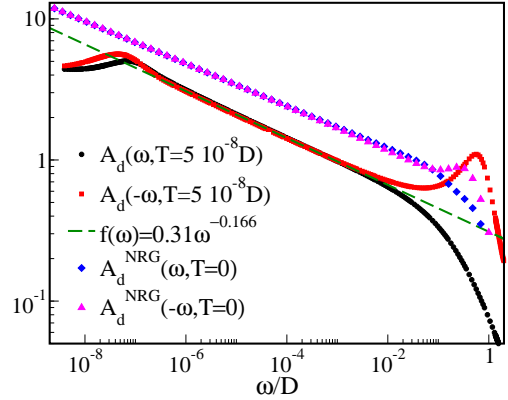


Figure 6 Impurity spectral function $A_d(\omega)$ for $r = 0.15$ very close to the critical fixed point (II) in Fig. 1, calculated using the NCA at temperature $T = 5 \times 10^{-8}D$ for $\epsilon_f/D = -0.6$ and $(V/D)^2 = 0.27$. Also shown is the spectral function calculated within the NRG for $T = 0$, $\epsilon_f/D = -0.1$ and $(V/D)^2 \simeq 0.0486$. The NCA and NRG spectral functions are described by very similar exponents (0.166 and 0.150, respectively), and both show that at the critical point, $A_d(\omega)$ is particle-hole symmetric at low energies.

tively vanishes. Obtaining converged numerical solutions near this fixed point is very difficult as the resulting sharp features cannot be resolved on discrete frequency grids. Increasing the hybridization V until a solution can be stabilized at the lowest accessible temperatures yields the critical solution (II) at $V = V_c$ where $(V_c/D)^2 \simeq 0.27$. Fig. 4 shows that the pseudoparticle exponents at this critical point agree well with the scaling ansatz results in Table 1. The temperature dependence of the static susceptibility reflects the frequency behavior. As a result, the dynamical local spin susceptibility $\chi(\omega, T)$ at the critical point exhibits the dynamical scaling form (see Fig. 5)

$$\chi(\omega, T) = T^{-x} \Phi(\omega/T), \quad (9)$$

with $x = 0.934$. It is instructive to compare this result against other methods. The NRG is unable to reliably access the regime $0 < |\omega|/T \ll 1$, so it cannot fully test for dynamical scaling. However, we find for the two-channel Kondo model with $r = 0.15$ that at the critical point, the NRG gives $\chi(\omega = 0, T) \propto T^{-x}$ and $\text{Im } \chi(\omega, T = 0) \propto |\omega|^{-y}$ with $x = y = 0.930 \pm 0.001$. These properties are entirely consistent with Eq. (9), and show that the NCA does an excellent job of calculating the exponent x . We note that this exponent deviates significantly from the leading-order value $x = 1 - 2r^2 = 0.955$ coming from an expansion about the local-moment fixed point [12].

Figure 6 shows the impurity spectral function $A_d(\omega)$ very close to the critical fixed point (II) in Table 1. The power-law variation is compatible with the $|\omega|^{-r}$ expected from the scaling ansatz, which coincides with the exact behavior known to hold at all intermediate-coupling fixed

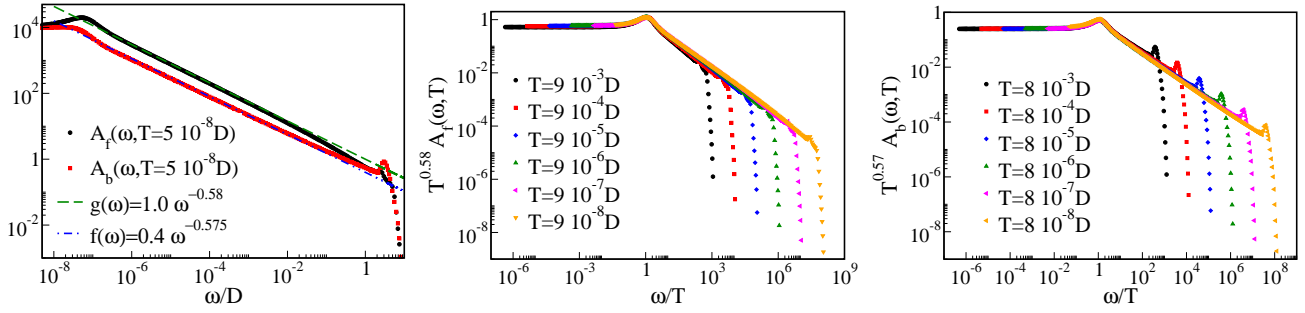


Figure 7 Pseudoparticle spectral functions $A_f(\omega, T)$ and $A_b(\omega, T)$ at the fixed point (III) in Fig. 1 for $r = 0.15$, $\epsilon_f/D = -0.6$, and $(V/D)^2 = 2.0$. (a) Frequency variation at $T = 5 \times 10^{-8}$. (b), (c) Dynamical scaling at different temperatures.

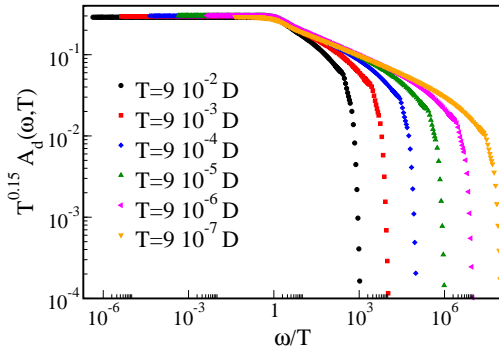


Figure 8 Dynamical scaling of the impurity spectral function $A_d(\omega, T)$ at the stable fixed point (III) in Fig. 1 for $r = 0.15$, $\epsilon_f/D = -0.6$, and $(V/D)^2 = 2.0$.

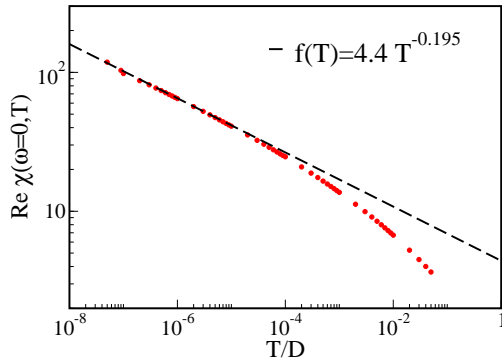


Figure 9 Static susceptibility χ vs temperature T at the stable fixed point (III) in Fig. 1 for $r = 0.15$, $\epsilon_f/D = -0.6$, and $(V/D)^2 = 2.0$.

points [12] and with the NRG results also plotted in Fig. 6. Both the NCA and the NRG show the critical spectral function to be particle-hole symmetric at small $|\omega|$.

The stable fixed point (III) in Table 1 can be accessed by increasing the hybridization beyond the critical value V_c . Figure 7 presents the pseudoparticle spectral functions at various temperatures for $(V/D)^2 = 2.0$. The threshold

exponents $\alpha_f = 0.58$ and $\alpha_b = 0.575$ extracted from Fig. 7(a) are in line with the prediction $\alpha_f = \alpha_b = (1+r)/2$ of the scaling ansatz. Figures 7(b) and 7(c) demonstrate that the temperature dependences of $A_f(\omega, T)$ and $A_b(\omega, T)$ are compatible with the frequency behavior such that dynamical, or ω/T -scaling ensues. This carries over to the impurity spectral function, which, as seen in Fig. 8, is compatible with the scaling

$$G_d^{\text{ret}}(\omega, T) = T^{-r} \Psi(\omega/T), \quad (10)$$

This scaling is consistent with the exact result [12] mentioned above, i.e., $A_d(\omega, T=0) \propto |\omega|^{-r}$.

Figure 9 plots the static local susceptibility vs temperature at the stable fixed point (III). A rather narrow window of asymptotic temperature dependence—presumably a consequence of a strong subleading contribution to $1/\chi(\omega=0, T)$ —gives an exponent $x = 0.195$ in reasonable agreement with the scaling ansatz prediction $x = 2\alpha_f - 1 = 0.15$.

Results for $r = 0.4$: We end this section by considering a representative case in the range $r_0 < r < 1$. For $r = 0.4$, the scaling ansatz predicts an asymmetric critical point described by $\alpha_f = \alpha_b = (1+r)/2 = 0.7$, the solution corresponding to (III) in Fig. 1. Figures 10 and 9 show results in the vicinity of this critical point, obtained for $\epsilon_f = -0.55D$ and $(V/D)^2 = 5.8$. The pseudoparticle exponents $\alpha_f = 0.7$, $\alpha_b = 0.68$ extracted from Fig. 10(a) closely follow the scaling ansatz, and the dynamical scaling of $A_d(\omega, T)$ with an exponent $0.37 \simeq r$ [Fig. 10(b)] agrees with the exact result [12]. Furthermore, the exponent $y = 0.44$ of $\chi(\omega, T=0) \propto |\omega|^{-y}$ fitted from the rather narrow frequency window of power-law behavior in Fig. 10(b) is in reasonable agreement with the value $y = x = 2\alpha_f - 1 = 0.4$ predicted by the scaling ansatz under the assumption of dynamical scaling and with $x = y = 0.381 \pm 0.001$ given by the NRG. The impurity spectral function, shown in Fig. 10(c), also appears to be consistent with dynamical scaling.

5 Conclusion We have investigated the reliability of the non-crossing approximation (NCA) for the two-

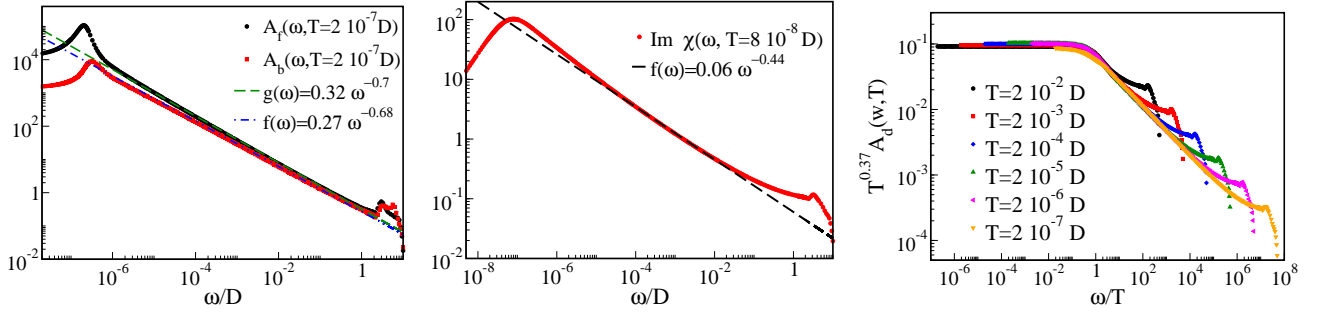


Figure 10 Results for $r = 0.4$ in the vicinity of the asymmetric critical point (III) in Fig. 1, calculated for $\epsilon_f = -0.55D$ and $(V/D)^2 = 5.8$. (a) Pseudoparticle spectral functions $A_f(\omega, T)$ and $A_b(\omega, T)$ at $T = 10^{-8}D$. (b) Dynamic spin susceptibility $\chi(\omega, T)$ at $T = 10^{-8}D$. (c) Dynamic scaling of the local density of states $A_d(\omega, T)$.

channel pseudogap Anderson model. This was accomplished by comparing finite-temperature, finite-frequency solutions of the NCA equations with asymptotically exact zero-temperature NCA solutions, with numerical renormalization-group calculations, and with exact results where available. In contrast to the well-known shortcomings of the NCA for the single-channel Anderson model with a constant density of states at the Fermi energy, the NCA captures surprisingly well the asymptotic low-energy properties of the two-channel model, both for metallic and semi-metallic (pseudogapped) hosts. In cases of a pseudogap, the results that we have presented for the magnetic susceptibility and the impurity spectral function are suggestive of frequency-over-temperature scaling in the dynamical properties. More complete testing for dynamical scaling is planned as future work. Finally, we note that the validation of the NCA treatment of this problem at equilibrium opens the way for its extension to nonequilibrium steady-state conditions [20].

Acknowledgements S.K. acknowledges support under NSF Grant No. PHYS-1066293 and the hospitality of the Aspen Center for Physics. Work at the U. of Florida was supported in part by the NSF MWN program under Grant No. DMR-1107814.

References

- [1] Q. Si, S. Rabello, K. Ingersent, and J. Smith, *Nature* **413**, 804 (2001).
- [2] P. Gegenwart, Q. Si, and F. Steglich, *Nat. Phys.* **4**, 186 (2008).
- [3] A. Schröder, G. Aeppli, R. Coldea, M. Adams, O. Stockert, H. v. Löhneysen, E. Bucher, R. Ramazashvili, and P. Coleman, *Nature* **407**, 351 (2000).
- [4] S. Friedemann, N. Oeschler, C. Krellner, C. Geibel, F. Steglich, S. Paschen, S. Kirchner, and Q. Si, *Proc. Natl. Acad. Sci. USA* **107**, 14547 (2010).
- [5] P. Coleman, *Phys. Rev. B* **29**, 3035 (1984).
- [6] E. Müller-Hartmann, *Z. Phys. B* **57**, 281 (1984).
- [7] B. Menge and E. Müller-Hartmann, *Z. Phys. B* **73**, 225 (1988).
- [8] D. L. Cox and A. L. Ruckenstein, *Phys. Rev. Lett.* **71**, 1613 (1993).
- [9] I. Affleck and A. Ludwig, *Phys. Rev. B* **48**, 7297 (1993).
- [10] T. A. Costi, P. Schmitteckert, J. Kroha, and P. Wölfle, *Phys. Rev. Lett.* **73**, 1275 (1994).
- [11] C. Gonzalez-Buxton and K. Ingersent, *Phys. Rev. B* **57**, 14254 (1998).
- [12] I. Schneider, L. Fritz, F. B. Anders, A. Benlarga, and M. Vojta, *Phys. Rev. B* **84**, 125139 (2011).
- [13] K. Sengupta and G. Baskaran, *Phys. Rev. B* **77**, 045417 (2008).
- [14] Z. G. Zhu, K. H. Ding, and J. Berakdar, *Eur. Phys. Lett.* **90**, 67001 (2010).
- [15] L. S. Mattos et al. (unpublished).
- [16] N. Read and D. Newns, *J. Phys. C: Solid State Phys.* **16**, L1055 (1983).
- [17] O. Parcollet and A. Georges, *Phys. Rev. B* **58**, 3794 (1998).
- [18] M. Vojta, *Phys. Rev. Lett.* **87**, 097202 (2001).
- [19] L. Zhu, S. Kirchner, Q. Si, and A. Georges, *Phys. Rev. Lett.* **93**, 267201 (2004).
- [20] F. Zamani et al. (in preparation).
- [21] S. Kirchner and J. Kroha, *J. Low Temp. Phys.* **126**, 1233 (2002).
- [22] S. Kirchner, J. Kroha, and P. Wölfle, *Phys. Rev. B* **70**, 165102 (2004).
- [23] Y. Kuramoto and H. Kojima, *Z. Phys. B* **57**, 95 (1984).
- [24] J. Kroha and P. Wölfle, *Act. Phys. Pol. B* **29**, 3781 (1998).
- [25] I. Affleck and A. W. W. Ludwig, *Nucl. Phys. B* **360**, 641 (1991).